

Dynamical defects in a two-dimensional Wigner crystal: self-doping and kinetic magnetism

Kyung-Su Kim,^{1,*} Ilya Esterlis,² Chaitanya Murthy,¹ and Steven A. Kivelson¹

¹*Department of Physics, Stanford University, Stanford, CA 93405*

²*Department of Physics, University of Wisconsin-Madison, Madison, Wisconsin 53706, USA*

(Dated: December 6, 2023)

We study the quantum dynamics of interstitials and vacancies in a two-dimensional Wigner crystal (WC) using a semi-classical instanton method that is asymptotically exact at low density, i.e., in the $r_s \rightarrow \infty$ limit. The dynamics of these point defects mediates magnetism with much higher energy scales than the exchange energies of the pure WC. Via exact diagonalization of the derived effective Hamiltonians in the single-defect sectors, we find the dynamical corrections to the defect energies. The resulting expression for the interstitial (vacancy) energy extrapolates to 0 at $r_s = r_{\text{mit}} \approx 70$ ($r_s \approx 30$), suggestive of a self-doping instability to a partially melted WC for some range of r_s below r_{mit} . We thus propose a “metallic electron crystal” phase of the two-dimensional electron gas at intermediate densities between a low density insulating WC and a high density Fermi fluid.

I. INTRODUCTION

Despite its prime importance in the field of condensed matter physics, some basic aspects remain unsettled concerning the physics of the two-dimensional electron gas (2DEG) at intermediate densities where various forms of “strongly correlated electron fluids” can arise. The ideal 2DEG is governed by the simple Hamiltonian

$$H = \sum_i \frac{\mathbf{p}_i^2}{2m} + \sum_{i < j} \frac{e^2}{4\pi\epsilon |\mathbf{r}_i - \mathbf{r}_j|}, \quad (1)$$

with a single dimensionless parameter, $r_s = a_0/a_B$, characterizing the ratio of the typical interaction strength to the kinetic energy. Here, $a_0 = 1/\sqrt{\pi n}$ is the average interparticle distance, n is the electron density, and $a_B = 4\pi\epsilon\hbar^2/me^2$ is the effective Bohr radius. The phases of the 2DEG in the weak and strong coupling limits are well-understood: it forms a paramagnetic Fermi liquid (FL) for small r_s (weak coupling) and a Wigner crystal (WC) for large r_s (strong coupling) [1]. The present study addresses the intermediate coupling regime near the quantum metal-insulator transition (MIT). Landmark numerical studies suggested that the MIT occurs as a direct transition from a Fermi liquid to an insulating WC at $r_s = r_{\text{melt}}^* \approx 31$ [2–4]. However, recent experiments [5–8] suggest that the actual transition may be more complex.

Apart from the charge ordering, there is another subtle issue regarding the magnetism. In the FL regime, the paramagnetic state seems to be most favored [4]. Deep within the WC phase, the magnetism is determined by various ring-exchange processes. The exchange coefficients can be calculated using the semi-classical instanton approximation [11–15], the validity of which is well-tested by a numerically exact path integral Monte

Carlo calculation [9]. These calculations show that the WC is a ferromagnet for large enough $r_s > r_{\text{F}}^{\text{wc}} \approx 175$ [9] and a (highly frustrated) antiferromagnet [13] below r_{F}^{wc} (Fig. 1). However, the predicted energy scale for the ring-exchange processes within the WC phase is too small to account for the typical magnetic energy scale of the insulating phase observed in the large r_s regime of various 2DEG systems [5, 7, 8]. This prompted some of the present authors to propose a kinetic mechanism that accounts for higher-temperature magnetism in such a phase mediated by interstitial hopping processes [16] [17].

In this paper, using the semi-classical instanton approximation, we carry out a comprehensive study of the quantum dynamics of an interstitial and a vacancy de-

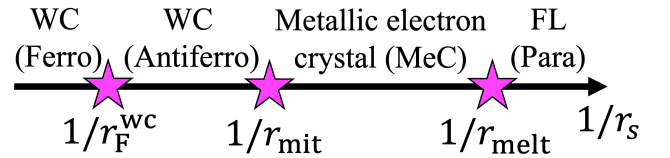


FIG. 1. Conjectured $T = 0$ phases of a clean 2DEG as a function of $1/r_s \propto \sqrt{n}$: WC (Ferro) = fully polarized ferromagnetic WC; WC (Antiferro) = WC with some form of antiferromagnetism (or a spin liquid phase); Metallic electron crystal (MeC) = metallic electron crystal characterized by more than one electron per unit cell; FL (Para) = paramagnetic Fermi liquid. The phase transition at $r_{\text{F}}^{\text{wc}} \approx 175$ [9] is due to the change of dominant exchange interactions from ferromagnetic to antiferromagnetic and is likely to be first order. $r_{\text{mit}} \approx 70$ indicates the “true” metal-insulator transition due to interstitial self-doping proposed in this paper, and is distinct from r_{melt} below which the crystalline order vanishes. r_{melt} is expected to be smaller than the value for a direct FL–WC transition from quantum Monte Carlo calculations, $r_{\text{melt}}^* \approx 31$ [4], due to the existence of the intermediate MeC phase. (Additional microemulsion phases may be expected [10] as well, especially for $r_s \sim r_{\text{melt}}^*$.) See Sec. IV for a detailed discussion of the conjectured phase diagram.

* Corresponding author.
kyungsu@stanford.edu

fect (Fig. 2), two point defects of a WC with the smallest classical creation energies [18, 19] [20]. We first review the formulation of the standard instanton technique and apply it to derive effective Hamiltonians describing various exchange and defect hopping processes illustrated in Fig. 4 (Sec. II). In Sec. III, we calculate the energy of an interstitial and a vacancy via finite-size exact diagonalization of the derived effective Hamiltonians. Interestingly, the resulting semi-classical expression for the interstitial energy, when extrapolated to a large but finite r_s , vanishes around $r_s = r_{\text{mit}} \approx 70$, signaling a possible self-doping instability to a partially melted WC below r_{mit} . From this, we propose the existence of a metallic electron crystal (MeC) phase as an intermediate phase of the 2DEG (Sec. IV). In Sec. V, we discuss the magnetic correlations induced by interstitial and vacancy hopping processes. Such kinetic processes induce magnetism with much higher energy scales than the ring-exchange processes of the pure WC; this could be experimentally probed by controlled doping of a WC that is commensurately locked to a weak periodic substrate potential. Our principal results are summarized in Figure 1. We conclude with a remark on the fate of the phase diagram in the presence of weak quenched disorder in Sec. VI.

II. THE SEMI-CLASSICAL APPROXIMATION

We first review the standard semi-classical instanton method as applied to the ideal 2DEG (1) in the large r_s limit. The exact partition function of the (fermionic) 2DEG is

$$Z = \int d^{2N} \mathbf{r}_0 \sum_{P \in S_N} \frac{(-1)^P}{N!} \sum_{\boldsymbol{\sigma}} \langle P \mathbf{r}_0, P \boldsymbol{\sigma} | e^{-\beta H} | \mathbf{r}_0, \boldsymbol{\sigma} \rangle, \quad (2)$$

$$\langle P \mathbf{r}_0, P \boldsymbol{\sigma} | e^{-\beta H} | \mathbf{r}_0, \boldsymbol{\sigma} \rangle = \delta_{\boldsymbol{\sigma}, P \boldsymbol{\sigma}} \langle P \mathbf{r}_0 | e^{-\beta H} | \mathbf{r}_0 \rangle, \quad (3)$$

$$\langle \mathbf{r}'_0 | e^{-\beta H} | \mathbf{r}_0 \rangle = \int_{\tilde{\mathbf{r}}(0)=\tilde{\mathbf{r}}_0}^{\tilde{\mathbf{r}}(\tilde{\beta})=\tilde{\mathbf{r}}'_0} D\tilde{\mathbf{r}}(\tau) e^{-\sqrt{r_s} S}, \quad (4)$$

$$S = \int_0^{\tilde{\beta}} d\tau \left[\frac{1}{2} \left(\frac{d\tilde{\mathbf{r}}}{d\tau} \right)^2 + V(\tilde{\mathbf{r}}) - V_0 \right], \quad (5)$$

$$V(\mathbf{r}) \equiv \sum_{i < j} \frac{1}{|\mathbf{r}_i - \mathbf{r}_j|}, \quad (6)$$

where $\mathbf{r}(\tau) \equiv \{\mathbf{r}_i(\tau)\}$ are the positions of N electrons in imaginary time, $\mathbf{r}_0 \equiv \{\mathbf{r}_i(\tau = 0)\}$ are their initial positions, $\boldsymbol{\sigma} \equiv \{\sigma_i = \uparrow, \downarrow\}$ are their respective spin indices, and $\beta = 1/k_B T$ is the inverse temperature. The sum over $N!$ permutations, P , of the coordinates and the sign factor $(-1)^P$ encode the fermionic exchange statistics. For bosonic particles, one should merely substitute $(-1)^P \rightarrow +1$. The 2DEG Hamiltonian (1) does not act on the electron spins, hence the $\delta_{\boldsymbol{\sigma}, P \boldsymbol{\sigma}}$ factor in the second line above. The third and fourth lines are the path integral representation of the N -electron

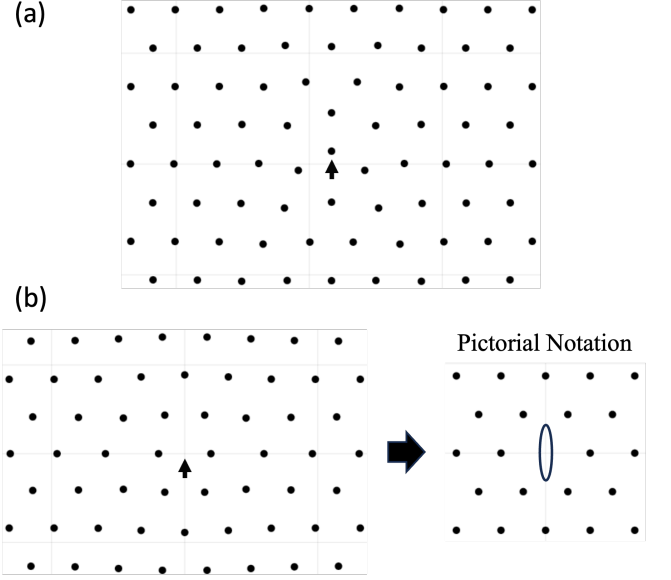


FIG. 2. (a) A classical centered interstitial and (b) a vacancy configuration. Small black arrows are drawn to indicate the positions of the interstitial (panel a) and the vacancy (left panel of b). The vacancy configuration has D_2 symmetry, and not the full D_6 symmetry of the underlying WC; therefore, a vacancy has three possible orientations α . We introduce a pictorial notation for the vacancy for later convenience.

propagator. The action is rescaled to make the r_s dependence manifest by introducing dimensionless coordinates, $\tilde{\mathbf{r}} \equiv \mathbf{r}/a_0$, and dimensionless imaginary time, τ . Correspondingly, $\tilde{\beta} \equiv \beta E^*$ is a dimensionless inverse temperature, where $E^* \equiv e^2/(4\pi\epsilon a_B r_s^{3/2})$. The path integral measure is also defined as an integration over the dimensionless coordinate $\tilde{\mathbf{r}}(\tau)$. The minimum potential energy $V_0 = \min_{\tilde{\mathbf{r}}} V(\tilde{\mathbf{r}})$ is subtracted for later convenience [21]. The Coulomb interaction (last line) is computed numerically using the standard Ewald method. As usual, the presence of a uniform neutralizing positively-charged background is assumed. Henceforth, we will drop tildes from the rescaled coordinates to simplify notation: $\tilde{\mathbf{r}} \rightarrow \mathbf{r}$. We focus on the zero temperature phase of the problem, and hence will always take $\beta \rightarrow \infty$ in the end.

We approach this problem using a semi-classical instanton approximation, which is asymptotically exact in the $r_s \rightarrow \infty$ (strong coupling) limit. In Sec. II A, we briefly review the semi-classical derivation of ring-exchange processes in the WC. In Sec. II B and II C, we consider tunneling processes involving a single interstitial and vacancy, respectively, and derive the corresponding effective Hamiltonians describing their dynamics. The application of the semi-classics to a bosonic system is addressed in Sec. II D.

A. Wigner crystal ring-exchange processes

In the $r_s \rightarrow \infty$ limit, the classical ground state manifold consists of a triangular lattice WC with 2^N -fold degeneracy in spin states. The lifting of this degeneracy and the nature of the resulting magnetic order is determined for $1 \ll r_s < \infty$ by WC ring-exchange processes. Various ring-exchange processes correspond to distinct instanton solutions of the action and can be calculated via the dilute instanton approximation [11–16, 22], which we briefly review below. (See Refs. [14, 15] for more details.) The result is an effective spin Hamiltonian expressed as a sum over all ring-exchange processes:

$$H_{\text{eff}}^{\text{wc}} = - \sum_a (-1)^{P_a} J_a (\hat{P}_a + \hat{P}_a^{-1}), \quad (7)$$

where the semi-classical calculation gives a leading-order large r_s asymptotic expression for J_a . Here, \hat{P}_a is the permutation operator corresponding to the permutation P_a , and can be decomposed as a product of two-particle exchange operators. The two-particle exchange operators, in turn, can be written in terms of spin operators as $\hat{P}_{(i,j)} = 2(\vec{S}_i \cdot \vec{S}_j + \frac{1}{4})$.

To illustrate how this works, recall the familiar problem of the semi-classical calculation of the tunnel splitting in a symmetric double-well potential [23–25]. For large enough β such that $\beta \hbar \omega_0 \gg 1$, the excited states in each well can be neglected. (Here, ω_0 is the oscillation frequency in either well.) In this limit, we obtain asymptotic relations

$$\langle \mathbf{r}_0 | e^{-\beta H} | \mathbf{r}_0 \rangle \sim |\psi(\mathbf{r}_0)|^2 e^{-\beta E_0} \cosh(\beta \Delta), \quad (8)$$

$$\langle -\mathbf{r}_0 | e^{-\beta H} | \mathbf{r}_0 \rangle \sim |\psi(\mathbf{r}_0)|^2 e^{-\beta E_0} \sinh(\beta \Delta), \quad (9)$$

where the minima of the two wells are at $\pm \mathbf{r}_0$, $|\psi(\mathbf{r}_0)|^2 = |\psi(-\mathbf{r}_0)|^2$ is the probability density of the wave function at these positions, and E_0 and 2Δ are, respectively, the mean energy and the splitting between the even and odd parity ground states. The right-hand side of each expression is obtained by inserting the resolution of the identity on the left-hand side.

In viewing this same problem from the path integral perspective in the semi-classical limit, one first solves for the instanton path—the smallest action path that begins at the bottom of one well and ends at the bottom of the other. The net duration (in imaginary time) of this tunneling event is of order ω_0^{-1} . We then sum over multiple such instanton events to obtain an expression of the same form as above, where the diagonal (off-diagonal) propagator in Eq. 8 (Eq. 9) contains all the terms with an even (odd) number of events. Expanding these expressions in power series, one sees that the typical number of tunneling events is $\sim \beta \Delta$ and the mean imaginary time interval between them is of order \hbar/Δ . Note that in the semi-classical limit $\hbar/\Delta \gg \omega_0^{-1}$, the instantons are dilute and hence effectively non-interacting (see Fig. 3). Looked at another way, for a range of temperature such

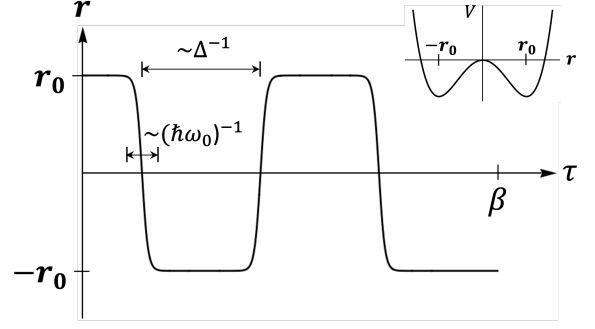


FIG. 3. An example of a multi-instanton configuration for the double well potential shown in the inset. The “size” of each instanton in imaginary time is $\sim 1/\hbar\omega_0$ and the “distance” between them is $\sim 1/\Delta$.

that $\hbar\omega_0 \gg T \gg \Delta$, where multiple instanton events can be neglected, we can compute Δ as

$$\Delta = \beta^{-1} \frac{\langle -\mathbf{r}_0 | e^{-\beta H} | \mathbf{r}_0 \rangle |_{1\text{-inst}}}{\langle \mathbf{r}_0 | e^{-\beta H} | \mathbf{r}_0 \rangle |_{0\text{-inst}}}, \quad (10)$$

where the subscripts designate the number of instanton events.

The analysis is somewhat more complicated but structurally similar for the present problem. Consider the propagator $\langle P_a \mathbf{r}_0 | e^{-\beta H} | \mathbf{r}_0 \rangle$ where \mathbf{r}_0 is an initial WC configuration and P_a is the permutation corresponding to a particular ring-exchange process [see Fig. 4(a)]. In the semi-classical (large r_s) limit, this propagator is again expressible as a weighted sum over multi-instanton contributions. For temperatures such that $\hbar\Omega \gg T \gg J_a$, where J_a is the tunnel splitting corresponding to the process P_a , the propagator is dominated (up to symmetry) by a single “a” instanton contribution associated with the path $\mathbf{r}^{(a)}(\tau)$ with the smallest action subject to the boundary conditions $\mathbf{r}^{(a)}(0) = \mathbf{r}_0$ and $\mathbf{r}^{(a)}(\beta) = P_a \mathbf{r}_0$. Here, $\hbar\Omega/2 \sim r_s^{-3/2}$ is the zero-point energy of the WC, while J_a is exponentially small in $\sqrt{r_s}$ at large r_s . The single- a -instanton contribution to the propagator can be expressed as

$$\begin{aligned} & \langle P_a \mathbf{r}_0 | e^{-\beta H} | \mathbf{r}_0 \rangle |_{a,1\text{-inst}} \\ & \approx e^{-\sqrt{r_s} S_a} \int_{\delta \mathbf{r}(0)=0}^{\delta \mathbf{r}(\beta)=0} D\delta \mathbf{r}(\tau) e^{-\frac{1}{2}\sqrt{r_s} \int_0^\beta \delta \mathbf{r}(\tau)^T \hat{\mathbf{M}}^{(a)}(\tau) \delta \mathbf{r}(\tau)} \\ & = e^{-\sqrt{r_s} S_a} \left(\det [\sqrt{r_s} \hat{\mathbf{M}}^{(a)}(\tau)] \right)^{-1/2}, \end{aligned} \quad (11)$$

$$\hat{M}_{ij}^{(a)}(\tau) \equiv \frac{\delta^2 S}{\delta r_i^{(a)}(\tau) \delta r_j^{(a)}(\tau)} = -\delta_{ij} \frac{\partial^2}{\partial \tau^2} + \partial_i \partial_j V[\mathbf{r}^{(a)}(\tau)], \quad (12)$$

where $S_a \equiv S[\mathbf{r}^{(a)}(\tau)]$ with the trajectory $\mathbf{r}^{(a)}(\tau)$ satisfying $\delta S[\mathbf{r}^{(a)}(\tau)] = 0$, and $\delta \mathbf{r}(\tau) \equiv \mathbf{r}(\tau) - \mathbf{r}^{(a)}(\tau)$ is the fluctuation coordinate. Fluctuations are treated within a harmonic approximation around the semi-classical path.

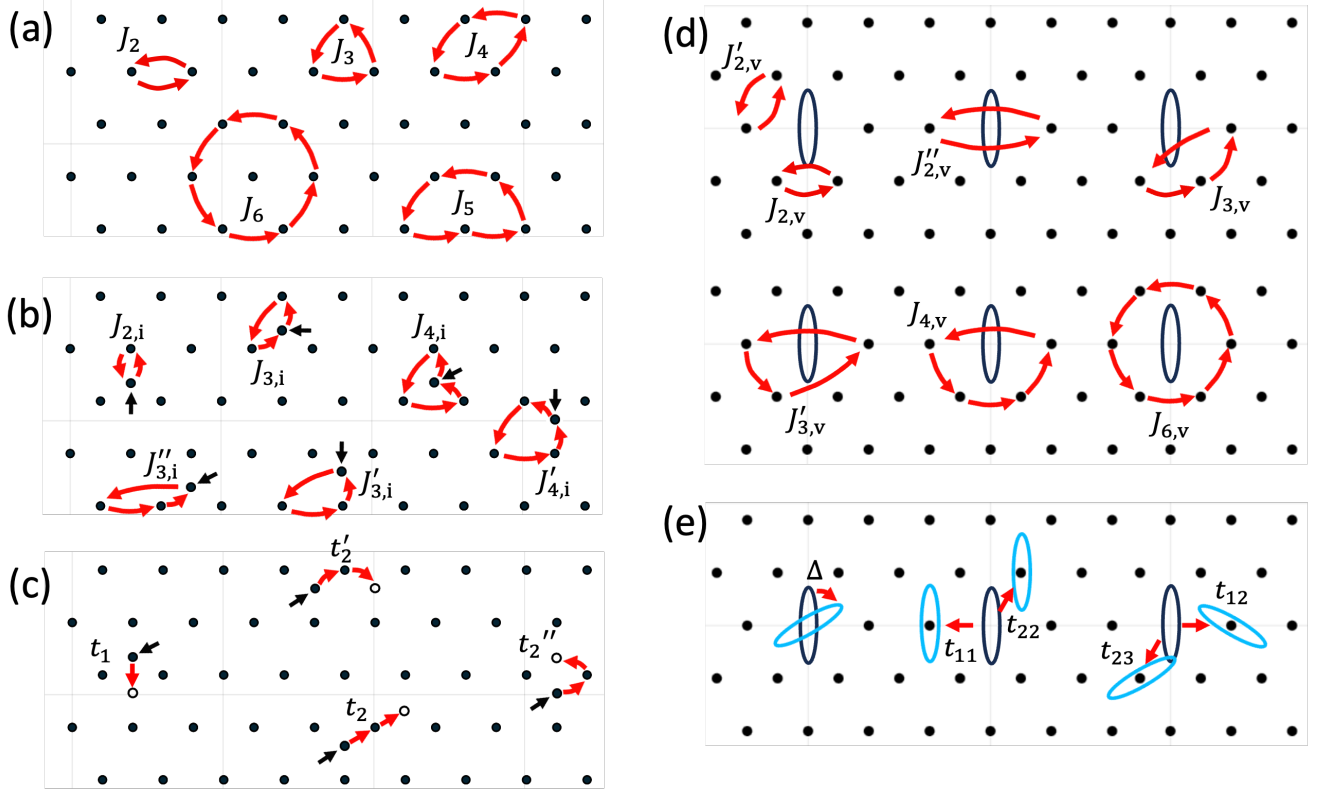


FIG. 4. Tunneling processes considered in this paper. (a) WC exchange processes. (b) Exchange processes involving an interstitial. (c) Interstitial hopping processes. (d) Exchange processes involving a vacancy. (e) Vacancy hopping processes. In (b,c), black arrows indicate the positions of interstitials. In (e), a black (cyan) oval denotes an initial (final) vacancy configuration corresponding to each vacancy hopping process. $t_{11}, t_{12}, t_{22}, t_{23}$ exhaust all the nearest-neighbor vacancy hopping processes; others are related to one of these by symmetry. Panels (a-c) are adapted from Ref. [16].

In Eq. (12), the derivative ∂_i is with respect to the normalized coordinates. Note that $\hat{\mathbf{M}}^{(a)}$ has a zero eigenvalue solution $\hat{\mathbf{r}}^{(a)}(\tau)$ corresponding to the translation in imaginary time, which has to be treated with care [14, 15, 23–25]. Separating the zero mode contribution from the full determinant, one obtains

$$\begin{aligned} & \langle P_a \mathbf{r}_0 | e^{-\beta H} | \mathbf{r}_0 \rangle |_{a,1\text{-inst}} \\ &= \beta \frac{e^2}{4\pi\epsilon a_B r_s^{3/2}} \sqrt{\frac{S_a}{2\pi}} \cdot e^{-\sqrt{r_s} S_a} \left(\det' [\sqrt{r_s} \hat{\mathbf{M}}^{(a)}(\tau)] \right)^{-\frac{1}{2}}, \end{aligned} \quad (13)$$

where the prime denotes that the zero eigenvalue must be omitted in the calculation of the determinant. Note that since an instanton is a localized object with a characteristic size $\Delta\tau = \Omega^{-1}$, one can neglect the exponentially small correction from its tail provided $\beta\hbar\Omega \gg 1$.

On the other hand, the diagonal propagator in the zero instanton sector $\langle \mathbf{r}_0 | e^{-\beta H} | \mathbf{r}_0 \rangle |_{0\text{-inst}}$ can be obtained by making a harmonic approximation of V around \mathbf{r}_0 :

$$\langle \mathbf{r}_0 | e^{-\beta H} | \mathbf{r}_0 \rangle |_{0\text{-inst}} \approx \left(\det [\sqrt{r_s} \hat{\mathbf{M}}^{(0)}(\tau)] \right)^{-\frac{1}{2}}, \quad (14)$$

$$\hat{M}^{(0)}(\tau) \equiv -\delta_{ij} \frac{\partial^2}{\partial \tau^2} + \partial_i \partial_j V(\mathbf{r}_0). \quad (15)$$

Normalizing the propagator in the one instanton sector by that in the zero instanton sector, as in Eq. (10), one obtains

$$\begin{aligned} J_a &= \beta^{-1} \frac{\langle P_a \mathbf{r}_0 | e^{-\beta H} | \mathbf{r}_0 \rangle |_{a,1\text{-inst}}}{\langle \mathbf{r}_0 | e^{-\beta H} | \mathbf{r}_0 \rangle |_{0\text{-inst}}} \\ &= \frac{e^2}{4\pi\epsilon a_B} \cdot \frac{A_a}{r_s^{5/4}} \sqrt{\frac{S_a}{2\pi}} e^{-\sqrt{r_s} S_a} > 0, \end{aligned} \quad (16)$$

$$A_a = \left[\frac{\det' (-\partial_\tau^2 + V''[\mathbf{r}^{(a)}(\tau)])}{\det (-\partial_\tau^2 + V''(\mathbf{r}_0))} \right]^{-\frac{1}{2}}, \quad (17)$$

where A_a is called a “fluctuation determinant,” calculated in the normalized coordinates with $r_s = 1$, and the $\beta \rightarrow \infty$ limit is implicitly taken in the end. In the second line, the extra factor of $r_s^{1/4}$ comes from the normalization of the determinant

$$\left(\frac{\det' [\sqrt{r_s} \hat{\mathbf{M}}^{(a)}(\tau)]}{\det [\sqrt{r_s} \hat{\mathbf{M}}^{(0)}(\tau)]} \right)^{-\frac{1}{2}} = r_s^{1/4} \left(\frac{\det' [\hat{\mathbf{M}}^{(a)}(\tau)]}{\det [\hat{\mathbf{M}}^{(0)}(\tau)]} \right)^{-\frac{1}{2}}.$$

Hence, A_a (17) (and also S_a) are dimensionless numbers with no r_s dependence. In Eq. (17), V'' denotes the hessian matrix of V . We refer readers to Appendix A for the

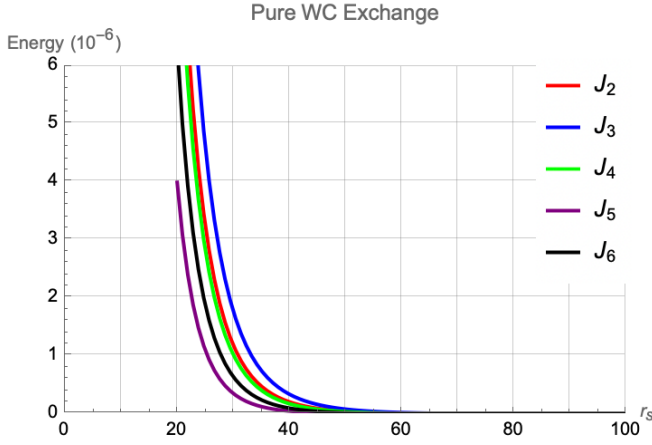


FIG. 5. Exchange coefficients of the pure WC (in units of the Hartree energy $e^2/4\pi\epsilon a_B$) as a function of r_s , calculated from the semi-classical expression (16). The processes corresponding to J_2, \dots, J_6 are schematically illustrated in Fig. 4(a). Within the WC phase ($r_s \gtrsim 30$), the instanton approximation is well-justified for the calculation of these ring-exchange processes since $\sqrt{r_s} S_a \gg 1$.

details of the numerical calculation of S_a and A_a . For the ring-exchange processes illustrated in Fig. 4(a), we quote the results for S_a and A_a from Ref. [15]: $S_2 = 1.64$, $A_2 = 1.30$; $S_3 = 1.53$, $A_3 = 1.10$; $S_4 = 1.66$, $A_4 = 1.24$; $S_5 = 1.91$, $A_5 = 1.57$; $S_6 = 1.78$, $A_6 = 1.45$. Our calculations, and those of Ref. [14], agree with these values. The resulting exchange coefficients calculated from the semi-classical expression (16) are shown in Fig. 5.

The remaining issue concerns the sign factor $(-1)^{P_a}$ that enters $H_{\text{eff}}^{\text{wc}}$ in Eq. (7), which is due to the anti-symmetry of the many-body electronic wave function (see chapter V of Ref. [12] for an explanation). As recognized by Thouless [22], this implies that a ring-exchange process involving an even (odd) number of electrons mediates an antiferromagnetic (ferromagnetic) interaction.

B. Processes involving a single interstitial

Tunneling processes involving a single centered interstitial (CI) defect [Fig. 2(a)] were first considered in Ref. [16]. We correct and refine the results obtained there: (1) The sign error in the correlated hopping terms t_2 and t'_2 in Eq. (4) of Ref. [16] is corrected in Eq. (18); (2) We improve the estimate of the classical action (which is done by solving the classical equations of motion for a finite sized system with periodic boundary conditions) using a hexagonal, instead of a rectangular, supercell with $12 \times 12 + 1$ electrons; and (3) We explicitly calculate the fluctuation determinants A_a rather than simply making dimensional estimates. Fig. 4(b-c) show the tunneling processes considered in this paper with the corresponding S_a and A_a listed in Table I. The hopping matrix elements $t_a > 0$ are again expressed in terms of S_a and A_a as in

Interstitial	S_a	A_a	Vacancy	S_a	A_a
t_1 (50,14)	0.098	0.23	Δ (50,12)	0.16	0.19
t_2 (50,14)	0.022	0.088	t_{11} (50,12)	0.011	0.050
t'_2 (50,12)	0.10	0.22	t_{22} (40,10)	0.31	0.19
t''_2 (50,12)	0.23	0.41	t_{12} (50,10)	0.13	0.091
$J_{2,i}$ (50,14)	0.37	0.26	t_{23} (60,12)	0.27	0.056
$J_{3,i}$ (50,12)	0.56	0.29	$J_{2,v}$ (50,16)	0.68	0.23
$J'_{3,i}$ (40,14)	0.69	0.32	$J'_{2,v}$ (30,12)	0.76	0.49
$J''_{3,i}$ (40,14)	0.82	0.26	$J''_{2,v}$ (50,16)	2.02	2.65
$J_{4,i}$ (40,14)	0.91	0.23	$J_{3,v}$ (50,16)	0.68	0.72
$J'_{4,i}$ (40,16)	0.54	0.69	$J'_{3,v}$ (30,16)	1.90	2.72
			$J_{4,v}$ (50,16)	0.66	0.58
			$J_{6,v}$ (50,16)	1.23	1.27

TABLE I. Dimensionless actions S_a and fluctuation determinants A_a for tunneling processes illustrated in Fig. 4(b-e) calculated in this paper. The parentheses in the first and fourth columns denote (N_{move}, M) , where N_{move} is the number of electrons that are allowed to adjust their positions during minimization and M is the number of time slices for the discretized tunneling paths (i.e., there are $M - 1$ intermediate configurations). Processes for a centered interstitial (vacancy) are calculated in a hexagonal supercell with $12 \times 12 + 1$ ($10 \times 10 - 1$) electrons starting and ending at fully relaxed defect configurations.

Eq. 16. Note that four hopping processes have smaller actions than those of exchange processes and hence are more important when $r_s \gg 1$. The effective Hamiltonian in the presence of a dilute concentration of interstitials is (corrected from Ref. [16])

$$\begin{aligned}
H_{\text{eff}}^i = & -t_1 \sum_{\langle n, n' \rangle} \sum_{\sigma} c_{n, \sigma}^{\dagger} c_{n', \sigma} \\
& -t_2 \sum_{\substack{(n, j, n') \\ \in (t_2 \text{ path})}} \sum_{\sigma, \sigma'} f_{j, \sigma}^{\dagger} c_{n, \sigma'}^{\dagger} f_{j, \sigma'} c_{n', \sigma} \\
& -t'_2 \sum_{\substack{(n, j, n') \\ \in (t'_2 \text{ path})}} \sum_{\sigma, \sigma'} f_{j, \sigma}^{\dagger} c_{n, \sigma'}^{\dagger} f_{j, \sigma'} c_{n', \sigma} \\
& -t''_2 \sum_{\substack{(n, j, n') \\ \in (t''_2 \text{ path})}} \sum_{\sigma, \sigma'} f_{j, \sigma}^{\dagger} c_{n, \sigma'}^{\dagger} f_{j, \sigma'} c_{n', \sigma} \\
& - \sum_{a \in (\text{CI ex.})} (-1)^{P_{a,i}} J_{a,i} (\hat{P}_{a,i} + \hat{P}_{a,i}^{-1}) \\
& + \dots + [U = \infty],
\end{aligned} \tag{18}$$

where $f_{j, \sigma}^{\dagger}$ ($c_{n, \sigma}^{\dagger}$) is the creation operator of electrons that live on the WC sites j (triangular plaquette centers n)

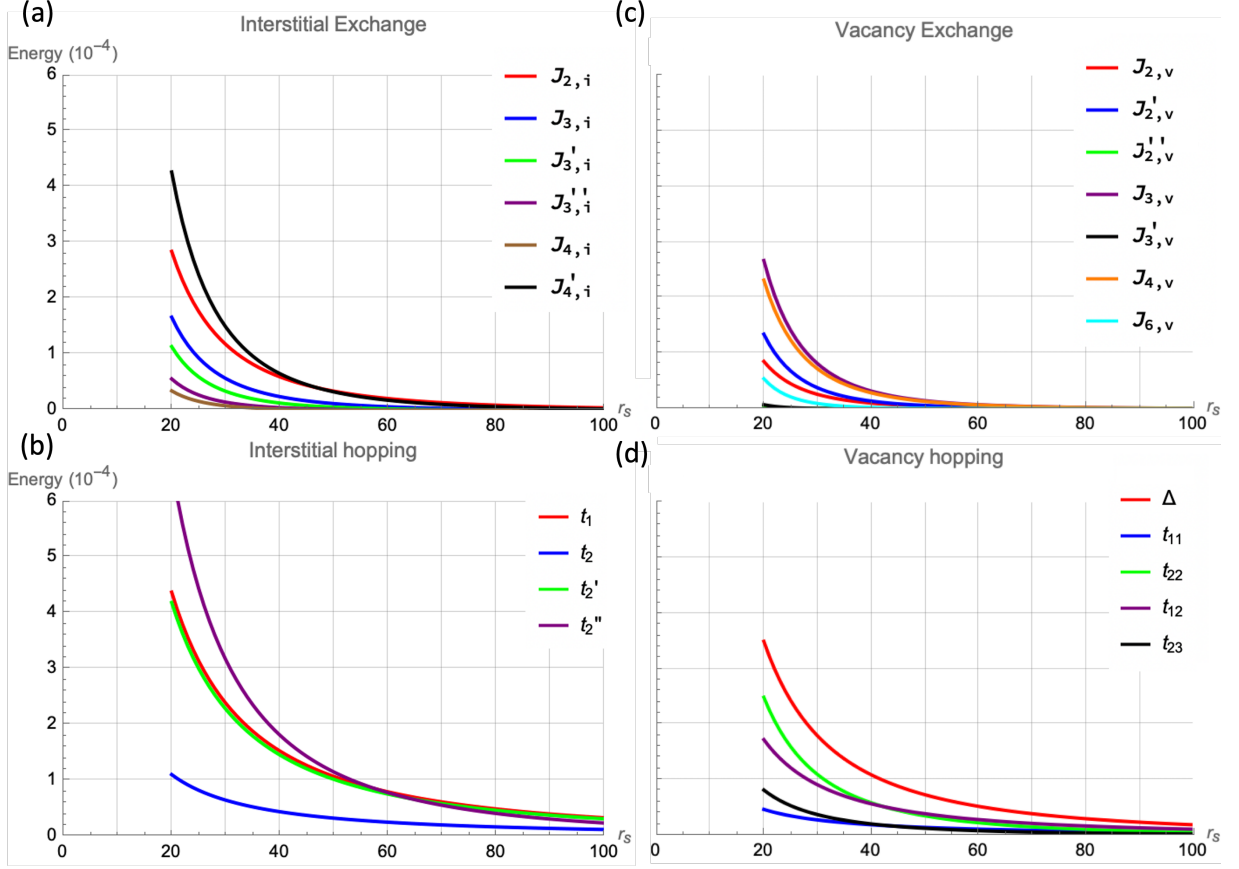


FIG. 6. Hopping matrix elements and exchange coefficients involving a defect (in units of $e^2/4\pi\epsilon a_B$) within the semi-classical approximation. Note that the y-axis scale here is a factor of 100 larger than in Fig. 5. Hence, the dynamical processes involving an interstitial or a vacancy have much larger energy scales than the exchange processes in the pure WC.

and the $U = \infty$ condition precludes any double occupancy. $\sigma, \sigma' = \uparrow, \downarrow$ are the spin indices that are summed over. $a \in (\text{CI ex.})$ denotes one of the exchange processes involving an interstitial shown in Fig. 4(b). The omitted terms correspond to hopping and exchange processes other than those shown in Fig. 4(b-c) and direct (elastic) interactions between interstitials [26]. Figure 6(a-b) shows the hopping matrix elements (t) and exchange coefficients (J) for processes involving an interstitial calculated from the semi-classical expression (16).

C. Processes involving a single vacancy

The classical vacancy defect has D_2 symmetry instead of the full D_6 symmetry of the underlying triangular lattice [19] [see Fig. 2(b)]. Therefore, associated with each location of a vacancy, there are 3 inequivalent orientations related by C_6 rotations. We will denote these by an index $\alpha = 1, 2, 3$; $\alpha = 2$ and 3 are related to $\alpha = 1$ by C_6 and C_6^2 respectively.

We considered tunneling processes involving a single vacancy defect as illustrated in Fig. 4(d-e), with their

corresponding values of S_a and A_a listed in Table I. The calculation is done in a hexagonal supercell containing $10 \times 10 - 1$ electrons. Again, matrix elements $\Delta, t_a, J_{a,v} > 0$ are given by Eq. (16) in terms of S_a and A_a . Note that, as in the interstitial case, the tunnel barriers (determined by S_a) for hopping processes are smaller than those for exchange processes [27].

The resulting effective Hamiltonian describing the dynamics of vacancies can be written straightforwardly as follows. First, corresponding to each orientation α of a vacancy, we introduce a (hard-core) bosonic operator $b_{i,\alpha}^\dagger$ that suitably relaxes the positions of the WC electrons near the vacancy site i to the associated configuration that minimizes the (classical) Coulomb energy. The operator that creates a vacancy in the WC at site i with orientation α is thus $f_{i,\sigma} b_{i,\alpha}^\dagger$. Then, with the definitions $\mathbf{b}_i^\dagger \equiv [b_{i,1}^\dagger, b_{i,2}^\dagger, b_{i,3}^\dagger]$ and

$$\mathfrak{D} \equiv \begin{bmatrix} 0 & \Delta & \Delta \\ \Delta & 0 & \Delta \\ \Delta & \Delta & 0 \end{bmatrix}, \quad \Upsilon \equiv \begin{bmatrix} t_{11} & t_{12} & t_{12} \\ t_{12} & t_{22} & t_{23} \\ t_{12} & t_{23} & t_{22} \end{bmatrix}, \quad \mathcal{C}_6 = \begin{bmatrix} 0 & 1 & 0 \\ 0 & 0 & 1 \\ 1 & 0 & 0 \end{bmatrix}, \quad (19)$$

the effective Hamiltonian in the presence of a dilute con-

centration of vacancies is

$$\begin{aligned}
H_{\text{eff}}^v = & - \sum_{i,\sigma} \left[\mathbf{b}_i^\dagger \mathfrak{D} \mathbf{b}_i + \sum_{\delta=\pm\mathbf{e}_1} f_{i,\sigma}^\dagger f_{i+\delta,\sigma} \mathbf{b}_{i+\delta}^\dagger \Upsilon \mathbf{b}_i \right. \\
& + \sum_{\delta=\pm\mathbf{e}_2} f_{i,\sigma}^\dagger f_{i+\delta,\sigma} \mathbf{b}_{i+\delta}^\dagger \mathcal{C}_6^{-1} \Upsilon \mathcal{C}_6 \mathbf{b}_i \\
& \left. + \sum_{\delta=\pm\mathbf{e}_3} f_{i,\sigma}^\dagger f_{i+\delta,\sigma} \mathbf{b}_{i+\delta}^\dagger \mathcal{C}_6^{-2} \Upsilon \mathcal{C}_6^2 \mathbf{b}_i \right] \\
& - \sum_{a \in (\text{V ex.})} (-1)^{P_{a,v}} J_{a,v} (\hat{P}_{a,v} + \hat{P}_{a,v}^{-1}) \\
& + \dots + [U = \infty], \tag{20}
\end{aligned}$$

where $\mathbf{e}_1 = [1, 0]$, $\mathbf{e}_2 = [1/2, \sqrt{3}/2]$, $\mathbf{e}_3 = [-1/2, \sqrt{3}/2]$, and $f_{i,\sigma}^\dagger$ is again the creation operator of an electron living at the WC site i . The first term describes on-site orientation-mixing processes corresponding to Δ ; the second term describes vacancy hopping processes in the $\pm\mathbf{e}_1$ directions; and the third (fourth) term describes vacancy hopping processes in the $\pm\mathbf{e}_2$ ($\pm\mathbf{e}_3$) directions, which can be related to the second term by \mathcal{C}_6 (\mathcal{C}_6^2) rotation [see Fig. 4(e)]. In the fifth term, $a \in (\text{V ex.})$ denotes one of the exchange processes around a vacancy shown in Fig. 4(d). The omitted terms correspond to hopping and exchange processes other than those shown in Fig. 4(d-e) and direct (elastic) interactions between vacancies [26]. Figures 6(c-d) shows the hopping matrix elements (t) and exchange coefficients (J) for processes involving a vacancy calculated from the semi-classical expression (16).

D. Two-Dimensional Bose Gas

For Coulomb-interacting bosonic particles, one merely needs to substitute $(-1)^{P_a} \rightarrow +1$ in $H_{\text{eff}}^{\text{wc}}$ (7) without changing the forms of H_{eff}^i and H_{eff}^v [(18) and (20)]. The consequence is that all ring-exchange processes and interstitial and vacancy hopping processes mediate ferromagnetism. This is a special case of a more general result that the ground state of an interacting multi-component bosonic system is a fully polarized ferromagnet [28, 29].

III. A SINGLE DEFECT: EXACT DIAGONALIZATION STUDY

In this section, we present the results of a finite-size exact diagonalization study (up to $3 \times 6 \pm 1$ electrons) of the derived effective Hamiltonians in the single-defect sector. (18,20) [30]. Figure 7 summarizes the result of the exact diagonalization calculation.

The maximum kinetic energy gain for an interstitial is calculated by obtaining the ground state of H_{eff}^i (18) in the single-interstitial sector. We retained all the terms shown in Fig. 4(b-c) except for $J_{3,i}''$ and $J_{4,i}$. (In the range of $20 \leq r_s \leq 100$ considered, they are more than

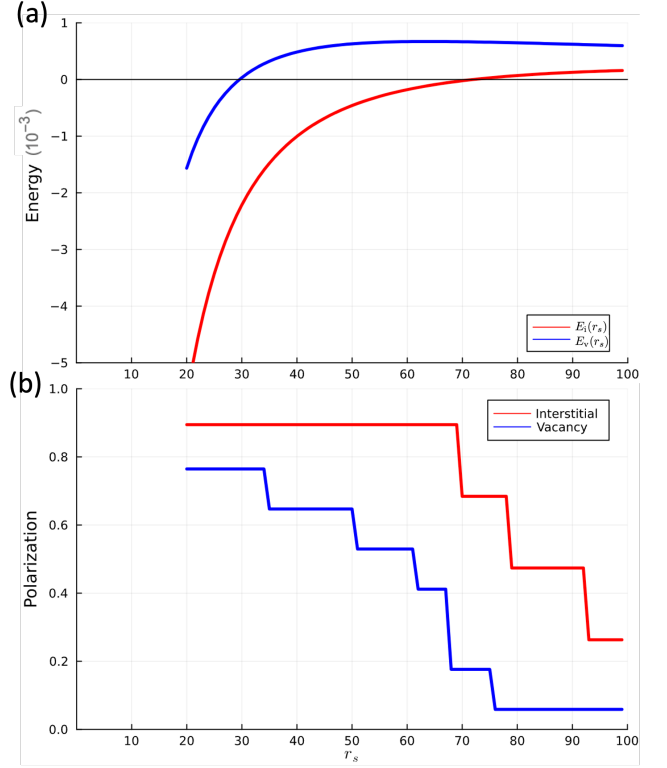


FIG. 7. Exact diagonalization results for the effective Hamiltonians (18, 23) on a 3×6 triangular lattice WC with periodic boundary conditions in the presence of a single defect. The semi-classical expressions (Fig. 6) are used as an input for the various matrix elements. (a) The ground state energy in the presence of a single interstitial (E_i) and a vacancy (E_v) as a function of r_s from the resulting semi-classical expressions (21, 25). $E_i(r_s)$ [$E_v(r_s)$] crosses zero around $r_s = r_{\text{mit}} \approx 70$ [$r_s \approx 30$]. (b) The relative spin polarization ($0 \leq 2S_{\text{tot}}^z/N_e \leq 1$) induced by a single interstitial and vacancy.

an order of magnitude smaller than the dominant terms in the Hamiltonian.) The resulting kinetic energy gain, $E_i^{\text{kin}}(r_s) < 0$, is calculated for a system of 3×6 WC sites with an additional interstitial (i.e., a total of $3 \times 6 + 1$ electrons) with periodic boundary conditions. Including the classical Coulomb energy and the zero-point vibrational energy, the minimum interstitial energy (in units of $e^2/4\pi\epsilon a_B$) is

$$E_i(r_s) = \frac{C_{1,i}}{r_s} + \frac{C_{3/2,i}}{r_s^{3/2}} + E_i^{\text{kin}}(r_s) + \dots \tag{21}$$

Here, we have neglected terms corresponding to higher order perturbative corrections (i.e., higher powers of $r_s^{-1/2}$) from phonon anharmonicity as well as higher order corrections to the semi-classical instanton approximation. We calculated $C_{1,i}$ and $C_{3/2,i}$ for supercells up to size $28 \times 28 + 1$; extrapolation to an infinite supercell size gives $C_{1,i} = 0.0769$ and $C_{3/2,i} = -0.295$ [31]. The semi-classical expression for the interstitial energy (21)

is plotted as a function of r_s in Fig. 7(a).

For the vacancy, the on-site orientation-mixing term Δ is the largest energy scale in the range of $20 \leq r_s \leq 100$, as shown in Fig. 6(c-d). Therefore, we simplify the vacancy problem by projecting it into the “isotropic single vacancy sector,” whose basis states are equal superpositions of all the vacancy orientations α at a site i :

$$\begin{aligned} |i; \{\sigma\}_{\text{wc}}\rangle &\equiv \frac{1}{\sqrt{3}} \sum_{\alpha=1}^3 |i, \alpha; \{\sigma\}_{\text{wc}}\rangle \\ &= \frac{1}{\sqrt{3}} \sum_{\alpha=1}^3 b_{i,\alpha}^\dagger f_{1,\sigma_1}^\dagger \cdots \cancel{f_{i,\sigma_i}^\dagger} \cdots f_{N,\sigma_N}^\dagger |\emptyset\rangle. \end{aligned} \quad (22)$$

Here $\{\sigma\}_{\text{wc}}$ are the spins of the WC electrons, and the slash in $\cancel{f_{i,\sigma_i}^\dagger}$ denotes that the corresponding operator is omitted from the product. The projection of $H_{\text{eff}}^{\text{v}}$ (20) to the isotropic single vacancy sector is straightforward, and yields

$$\begin{aligned} H_{\text{eff}}^{\text{v}}|_{\Delta} &= -2\Delta - t_{\Delta}^{\text{eff}} \sum_{\langle i,j \rangle} (f_{i,\sigma}^\dagger f_{j,\sigma} + \text{H.c.}) \\ &+ \sum_i (1 - n_i) \left[J_2^{\text{eff}} \sum_{\langle j,k \rangle} \hat{P}_{j,k} - J_3^{\text{eff}} \sum_{\langle j,k,l \rangle} \hat{P}_{j,k,l} \right. \\ &\quad \left. + J_4^{\text{eff}} \sum_{\langle j,k,l,m \rangle} \hat{P}_{j,k,l,m} + \text{H.c.} \right], \end{aligned} \quad (23)$$

where

$$\begin{aligned} t_{\Delta}^{\text{eff}} &\equiv \frac{1}{3} [1, 1, 1] \Upsilon \begin{bmatrix} 1 \\ 1 \\ 1 \end{bmatrix} = \frac{1}{3} (t_{11} + 2t_{22} + 4t_{12} + 2t_{23}), \\ J_2^{\text{eff}} &\equiv \frac{1}{3} (J_{2,\text{v}} + 2J'_{2,\text{v}} + \frac{1}{2} J''_{2,\text{v}}), \\ J_3^{\text{eff}} &\equiv \frac{2}{3} (J_{3,\text{v}} + J'_{3,\text{v}}), \quad J_4^{\text{eff}} \equiv \frac{1}{3} J_{4,\text{v}}. \end{aligned} \quad (24)$$

In the presence of N_{v} isotropic vacancies, one substitutes $2\Delta \rightarrow 2N_{\text{v}}\Delta$. The $(1 - n_i)$ factor locates the vacancy, where $n_i = \sum_{\sigma} f_{i,\sigma}^\dagger f_{i,\sigma}$, and $\langle j, k \rangle$, $\langle j, k, l \rangle$ and $\langle j, k, l, m \rangle$ are the 2, 3, and 4 sites neighboring the vacancy location i participating in the corresponding ring-exchange processes (j, k, l, m themselves are also nearest neighbors). $J'_{2,\text{v}}, J'_{3,\text{v}}, J_{6,\text{v}}$ are much smaller than other terms in $H_{\text{eff}}^{\text{v}}$ and hence will be ignored.

By solving $H_{\text{eff}}^{\text{v}}|_{\Delta}$ (23) in the single vacancy sector, we numerically find the minimum possible vacancy kinetic energy, $E_{\text{v}}^{\text{kin}}(r_s) < 0$, on 3×6 WC sites in the presence of a single vacancy ($3 \times 6 - 1$ electrons). The full semi-classical expression, including the Coulomb and zero-point energy, for the vacancy energy (in units of $e^2/4\pi\epsilon a_{\text{B}}$) is then

$$E_{\text{v}}(r_s) = \frac{C_{1,\text{v}}}{r_s} + \frac{C_{3/2,\text{v}}}{r_s^{3/2}} + E_{\text{v}}^{\text{kin}}(r_s) + \cdots, \quad (25)$$

where, again, the neglected terms correspond to higher order perturbative and non-perturbative corrections. We

calculated $C_{1,\text{v}}$ and $C_{3/2,\text{v}}$ for supercells up to $24 \times 24 - 1$; extrapolation to an infinite supercell size gives $C_{1,\text{v}} = 0.1094$ and $C_{3/2,\text{v}} = -0.368$. Whereas our result for $C_{1,\text{v}}$ agrees with Ref. [19] up to the fourth digit, our value for $C_{3/2,\text{v}}$ is slightly different from theirs [32]. The semi-classical expression for the vacancy energy (25) is plotted as a function of r_s in Fig. 7(a).

Note that due to the presence of small competing exchange interactions of the underlying WC, a single defect will induce magnetism only in a finite region around it, forming a magnetic polaron. Such a competition effectively increases the energy of an interstitial and a vacancy by a small amount as measured relative to the energy of the pure WC.

The semi-classical expressions for the interstitial (vacancy) energy vanishes around $r_s = r_{\text{mit}} \approx 70$ ($r_s \approx 30$), indicating a possible instability of the WC to interstitial self-doping for $r_s < r_{\text{mit}}$ (Fig. 7).

IV. INTERMEDIATE PHASES OF THE 2DEG

Our predicted value of $r_{\text{mit}} \approx 70$ is larger than $r_{\text{melt}}^* \approx 31$, where r_{melt}^* is the value below which—according to existing variational calculations—the energy of the paramagnetic Fermi liquid becomes smaller than the energy of a WC (with a particular assumed antiferromagnetic order) [4]. This suggests that there is a range of densities, $r_{\text{melt}} < r_s < r_{\text{mit}}$, for which a metallic electron crystal (MeC) phase with more than one electron per crystalline unit cell is stable [33]. Here, r_{melt} is the value below which the crystalline order vanishes (see Fig. 1). (We expect $r_{\text{melt}} < r_{\text{MIT}}^* \approx 31$ because our metallic WC phase is expected to have a lower energy than the pure WC.) To the best of our knowledge, the proposed MeC phase with more than one electron per crystalline unit cell has not been studied using the variational quantum Monte Carlo method. A related, but distinct, MeC phase with less than one electron per crystalline unit cell has been studied in Refs. [34] and [4]; however, these studies are in disagreement with each other.

As discussed in the next section, an interstitial forms a large magnetic polaron in a WC, so the MeC phase occurring near r_{mit} (Fig. 1) is expected to be characterized by an anomalously large quasi-particle (interstitial) effective mass. Such massive magnetic polarons have a tendency to agglomerate, leading to phase separation [35–37] and rendering the transition at r_{mit} to be first-order [38]. Note that for single component (spinless) electrons, polaron formation is not an issue so the self-doping transition may be continuous [39].

Finally, the transition to a fully melted Fermi fluid occurs when the energy of the MeC phase crosses that of the liquid phase. Existing variational quantum Monte Carlo estimates of the critical r_s involve comparing the energy of the liquid to that of the insulating WC. If, as we have suggested, the MeC has lower energy than the insulating WC in an intermediate r_s regime, it would presumably

be stable against quantum melting at somewhat higher densities (smaller r_s). Thus, this carries with it the likely implication that $r_{\text{melt}} < r_{\text{melt}}^* \approx 31$.

V. KINETIC MAGNETISM

Here, we discuss the magnetic correlations induced by defect hopping processes [40].

Distinct interstitial hopping terms induce different magnetic correlations in the underlying WC. The character of the dominant magnetic correlations induced by each hopping process is determined by the parity of the smallest spin permutation it induces [22]. For example, by applying t_2'' terms twice on the interstitial, one recovers the same charge configuration but with 3 electrons (spins) permuted. This is an even permutation and mediates ferromagnetism as discussed in Sec. II A. Similarly, the smallest permutation that the t_2 terms induce involves 7 electrons (even permutation) and also mediates ferromagnetism. On the other hand, the smallest spin permutation induced by t_2' process involves 4 electrons (odd permutation) and mediates antiferromagnetism. The t_1 hopping term does not couple with the underlying WC and hence does not induce magnetism by itself. Taken together, the various hopping terms, in combination with exchange processes $J_{a,i}$, lead to a complicated problem with competing magnetic tendencies.

Interestingly, the interstitial dynamics induces non-trivial spin polarization $2S_{\text{tot}}^z/N_e$, as shown in Fig. 7(b), where S_{tot}^z is the total S^z quantum number and N_e is the number of electrons in the system. For $20 \leq r_s < 70$, the interstitial seems to always favor a single spin-flip in a fully polarized background (this is also true for smaller systems of $3 \times 4 + 1$ or $3 \times 5 + 1$ electrons) [41].

In the presence of small antiferromagnetic WC exchange interactions, a single interstitial can only delocalize in a finite region, forming a large magnetic polaron of size $\sim a_0^2 \sqrt{t/J}$ [16, 35, 42], where t and J are characteristic values of interstitial hopping matrix elements and WC exchange coefficients, respectively. At $r_s \approx 45$, we estimate that a single interstitial induces a magnetic polaron involving ~ 40 WC spins.

On the other hand, it is known that the dynamics of a single hole in the $U = \infty$ Hubbard model on a non-bipartite lattice leads to some form of antiferromagnetism [43–47]; therefore, assuming that the isotropic vacancy is energetically favored, its hopping processes mediate antiferromagnetic correlations around it. In the presence of competing exchange interactions of the underlying WC, a vacancy similarly forms a finite-sized antiferromagnetic polaron.

By controlled doping of a WC in the presence of a smoothly varying weak external periodic potential, one can obtain the defect-doped commensurate WC phase as a stable ground state, as the following reasoning shows. Consider a weak commensurate potential that has minima $-W < 0$ at the triangular lattice WC sites.

When the density is tuned away (but not too far away) from the commensurate value, the defect-doped commensurate WC has an energy per electron $\Delta E_{\text{comm}}/N \approx -W + E_{\text{def}}|\delta| + O(W|\delta|, \delta^2)$ as compared to the pure incommensurate WC, where δ is the ratio of defect electrons to the total number of electrons, and $E_{\text{def}} = E_i$ (E_v) is the energy of an interstitial (vacancy) defect in the absence of the external potential. Therefore, for a range of doping $-W/E_v < \delta < W/E_i$, the system will form a defect-doped metallic WC phase that is commensurately locked to the external potential. Such a phase, in turn, is characterized by defect-induced magnetic correlations with much higher energy scales than the exchange processes of the pure WC. Therefore, one expects that the magnetic energy scale increases as one moves away from the commensurate filling. Such a proposal may be experimentally tested in certain Moiré systems that support a commensurately locked WC phase [48–52].

VI. EFFECTS OF WEAK DISORDER

Before concluding, we remark on the effect of small quenched disorder on the phase diagram (Fig. 1). Firstly, even weak disorder is expected to destroy any long-range crystalline order; hence all the electronic crystalline states we have discussed are defined only in an approximate sense as short-range ordered states. Also, the MeC phase is characterized by the reduced density of mobile electrons and their increased effective mass; hence, even weak disorder is likely to result in strong localization and destroy the metallic character of the phase. The resulting disorder-induced intermediate insulating phase is characterized by large magnetic energy scales, associated with the dynamical processes of defects. This may be an explanation for the recently observed insulating phases with much higher magnetic energy than the exchange scales of the pure WC [5, 7, 8]. Note that such a proposal predicts an exponential reduction of magnetic energy scales with increasing r_s for $r_s > r_{\text{mit}}$ [53].

ACKNOWLEDGEMENT

We thank Boris Spivak for initial insights which led to this investigation and Akshat Pandey for collaboration on a previous work. We appreciate Veit Elser, Brian Skinner and Shafayat Hossain for interesting comments on the draft. K-S.K. acknowledges the hospitality of the Massachusetts Institute of Technology, where this work was completed, and thanks Aidan Reddy, Seth Musser and Yubo Paul Yang for helpful discussions. I.E. acknowledges Eugene Demler, Hongkun Park, Jiho Sung, Pavel Volkov, Jue Wang, and Yubo Yang for helpful discussions on related work. K-S.K. and SAK were supported in part by the Department of Energy, Office of Basic Energy Sciences, Division of Materials Sciences and Engineering, under contract DE-AC02-76SF00515

at Stanford. I.E. was supported by AFOSR Grant No. FA9550-21-1-0216 and the University of Wisconsin-Madison. C.M. was supported in part by the Gordon and Betty Moore Foundation's EPiQS Initiative through GBMF8686, and in part by the National Science Foundation under Grants No. NSF PHY-1748958 and PHY-2309135. Parts of the computing for this project were performed on the Sherlock computing cluster at Stanford University.

Appendix A: Numerical calculations of S and A

In this section, we review a numerical method for calculating S_a (5) and A_a (17), closely following Ref. [15]. Although we applied the semi-classical instanton calculation to the 2DEG specifically, the method outlined here applies to any system with a general potential $V(\mathbf{r})$ with degenerate minima in the semi-classical limit. We first calculate the instanton action S_a (5) by discretizing a

tunneling path:

$$S_a = \int_{\mathbf{r}_0}^{\mathbf{r}'_0} d\mathbf{r} \sqrt{2\Delta V(\mathbf{r})} \quad (\text{A1})$$

$$\approx \sum_{k=1}^{N_{\text{time}}} \frac{1}{2} |\mathbf{r}_k - \mathbf{r}_{k-1}| \cdot [\sqrt{2\Delta V(\mathbf{r}_k)} + \sqrt{2\Delta V(\mathbf{r}_{k-1})}],$$

where we defined $\Delta V(\mathbf{r}) \equiv V(\mathbf{r}) - V(\mathbf{r}_0)$ and used the semi-classical equation of motion $\ddot{\mathbf{r}} = \nabla V(\mathbf{r})$. \mathbf{r}_0 and \mathbf{r}'_0 are initial and final minimum configurations of V , respectively, $\mathbf{r}_k \equiv \mathbf{r}(\tau_k)$ is the collective coordinate of particles at time τ_k , where $0 \equiv \tau_0 < \tau_1 < \tau_2 < \dots < \tau_M \equiv \tilde{\beta}$, and $\mathbf{r}_M \equiv \mathbf{r}'_0$. In order to make the distances $|\mathbf{r}_k - \mathbf{r}_{k-1}|$ approximately equal, each \mathbf{r}_k is taken to be constrained in the hyperplane defined by $(\mathbf{r}_k - \mathbf{r}_0) \cdot (\mathbf{r}'_0 - \mathbf{r}_0) = \frac{k}{M} |\mathbf{r}'_0 - \mathbf{r}_0|^2$. Numerical minimization of the discretized action (A1) is performed with a standard optimization package [54]. We will henceforth denote by \mathbf{r}_k ($k = 0, 1, \dots, M$) the optimized tunneling path for the a -instanton process.

The fluctuation determinant A_a captures the Gaussian fluctuations around the semi-classical path

$$A_a = \frac{F'[\mathbf{r}^{(a)}(\tau)]}{F[\mathbf{r}_0]} = \left[\frac{\det'(-\partial_\tau^2 + V''[\mathbf{r}^{(a)}(\tau)])}{\det(-\partial_\tau^2 + V''(\mathbf{r}_0))} \right]^{-\frac{1}{2}}, \quad (\text{A2})$$

$$F[\mathbf{r}(\tau)] \equiv \int_{\delta\mathbf{r}(0)=0}^{\delta\mathbf{r}(\tilde{\beta})=0} D\delta\mathbf{r}(\tau) \exp \left[-\frac{1}{2} \int_0^{\tilde{\beta}} \left(\delta\dot{\mathbf{r}}(\tau)^2 + \delta\mathbf{r}(\tau)^T V''[\mathbf{r}^{(a)}(\tau)] \delta\mathbf{r}(\tau) \right) d\tau \right] = \langle \mathbf{0} | \mathcal{T} \exp(-\int_0^{\tilde{\beta}} d\tau h[\mathbf{r}^{(a)}(\tau)]) | \mathbf{0} \rangle, \quad (\text{A3})$$

$$h[\mathbf{r}(\tau)] \equiv -\frac{1}{2} \nabla^2 + \frac{1}{2} \delta\mathbf{r}(\tau)^T V''[\mathbf{r}(\tau)] \delta\mathbf{r}(\tau), \quad (\text{A4})$$

where $\mathcal{T} \exp(\dots)$ denotes the imaginary-time-ordered exponential, $\delta\mathbf{r}(\tau) \equiv \mathbf{r}(\tau) - \mathbf{r}^{(a)}(\tau)$ is the fluctuation coordinate, and the primed determinant in the first line is again computed with the zero mode omitted. $\tilde{\beta} \rightarrow \infty$ is implicitly taken in the end in calculating A_a . As discussed below, the calculation of A_a can be done numerically by first computing $F[\mathbf{r}^{(a)}(\tau)]/F[\mathbf{r}_0]$ that includes the zero mode contribution, and then multiplying by the square root of the smallest eigenvalue (which is exponentially small in $\tilde{\beta}$) of the operator $-\partial_\tau^2 + V''[\mathbf{r}^{(a)}(\tau)]$.

$F[\mathbf{r}^{(a)}(\tau)]$ can be calculated by discretizing the path integral expression (A3). First, we further define the time slices intermediate to those defined above

$$0 < \tau_{1/2} < \tau_1 < \tau_{1+1/2} < \dots < \tau_{M-1/2} < \tau_M \equiv \tilde{\beta}, \quad (\text{A5})$$

where each interval, $\Delta\tau_k \equiv \tau_{k+1/2} - \tau_{k-1/2}$ ($k = 1, \dots, M-1$), is calculated by inverting the semi-classical equation of motion

$$\Delta\tau_k \equiv \int_{\mathbf{r}_{k-1/2}}^{\mathbf{r}_{k+1/2}} \frac{d\mathbf{r}}{\sqrt{2\Delta V[\mathbf{r}^{(a)}(\tau)]}} \approx \frac{1}{\sqrt{2\Delta V(\mathbf{r}_k)}} \cdot \frac{1}{2} (|\mathbf{r}_{k+1} - \mathbf{r}_k| + |\mathbf{r}_k - \mathbf{r}_{k-1}|), \quad (\text{A6})$$

and analogously for the end intervals, $\Delta\tau_0 \equiv \tau_{1/2} \approx \frac{1}{\sqrt{2\Delta V(\mathbf{r}_0)}} \cdot \frac{1}{2} |\mathbf{r}_1 - \mathbf{r}_0|$ and $\Delta\tau_M \equiv \tau_M - \tau_{M-1/2} \approx \frac{1}{\sqrt{2\Delta V(\mathbf{r}_M)}} \cdot \frac{1}{2} |\mathbf{r}_M - \mathbf{r}_{M-1/2}|$. (Note that the end intervals formally diverge, $\Delta\tau_{0,M} \rightarrow \infty$, as $\tilde{\beta} \rightarrow \infty$.) Then, the propagator at each interval can be approximated by that of the quantum harmonic oscillator (Mehler kernel) of $h[\mathbf{r}^{(a)}(\tau)] \approx h_k \equiv h[\mathbf{r}_k]$

$$\left\langle \delta \mathbf{r}_{k+\frac{1}{2}} \left| e^{-\Delta \tau_k h_k} \right| \delta \mathbf{r}_{k-\frac{1}{2}} \right\rangle = \prod_{n=1}^{2N} \left(\sqrt{B_{n,k}^{(a)}} \exp[-S_{n,k}^{(a)}] \right), \quad (\text{A7})$$

$$S_{n,k}^{(a)} = \frac{A_{n,k}^{(a)}}{2} \left[\left\langle \mathbf{v}_{n,k} \left| \delta \mathbf{r}_{k-\frac{1}{2}} \right\rangle^2 + \left\langle \mathbf{v}_{n,k} \left| \delta \mathbf{r}_{k+\frac{1}{2}} \right\rangle^2 \right] - B_{n,k}^{(a)} \left\langle \mathbf{v}_{n,k} \left| \delta \mathbf{r}_{k-\frac{1}{2}} \right\rangle \left\langle \mathbf{v}_{n,k} \left| \delta \mathbf{r}_{k+\frac{1}{2}} \right\rangle \right], \quad (\text{A8})$$

where

$$V''(\mathbf{r}_k) \mathbf{v}_{n,k} \equiv (\omega_{n,k})^2 \mathbf{v}_{n,k}, \quad (n = 1, \dots, 2N), \quad (\text{A9})$$

$$A_{n,k}^{(a)} \equiv \frac{\omega_{n,k}}{\tanh(\omega_{n,k} \Delta \tau_k)}, \quad B_{n,k}^{(a)} \equiv \frac{\omega_{n,k}}{\sinh(\omega_{n,k} \Delta \tau_k)}. \quad (\text{A10})$$

Eq. A9 defines normal mode frequencies and eigenmodes at each time slice k . Note that at intermediate times $k \neq 0, M$, $\omega_{n,k}$ is in general complex. At the end in-

tervals $k = 0, M$, one substitutes $\delta \mathbf{r}_{-\frac{1}{2}} \rightarrow \delta \mathbf{r}_0 = 0$ and $\delta \mathbf{r}_{M+\frac{1}{2}} \rightarrow \delta \mathbf{r}_M = 0$ in the above expressions. (Note that as $\tilde{\beta} \rightarrow \infty$, the propagators at the end intervals approach zero exponentially. However, as we will see below, such contributions cancel when calculating A_a as we are calculating the ratio between two F s.)

$F[\mathbf{r}^{(a)}(\tau)]$ can finally be computed by integrating over the intermediate fluctuation coordinates $\delta \mathbf{r}_{k-\frac{1}{2}}$

$$\begin{aligned} F[\mathbf{r}^{(a)}(\tau)] &= \int \left(\prod_{k=1}^M d^{2N} \delta \mathbf{r}_{k-\frac{1}{2}} \right) \left\langle \mathbf{0} \left| e^{-\Delta \tau_M h_M} \right| \delta \mathbf{r}_{M-\frac{1}{2}} \right\rangle \left\langle \delta \mathbf{r}_{M-\frac{1}{2}} \left| e^{-\Delta \tau_{M-1} h_{M-1}} \right| \delta \mathbf{r}_{M-\frac{3}{2}} \right\rangle \cdots \left\langle \delta \mathbf{r}_{\frac{1}{2}} \left| e^{-\Delta \tau_0 h_0} \right| \mathbf{0} \right\rangle \\ &= \left(\prod_{k=0}^M \prod_{n=1}^{2N} \sqrt{B_{n,k}^{(a)}} \right) \det(\mathcal{M}^{(a)})^{-\frac{1}{2}}, \end{aligned} \quad (\text{A11})$$

$$\begin{aligned} \mathcal{M}^{(a)} &\equiv \sum_{k=1}^M e_{k,k} \otimes (\mathcal{A}_{k-1}^{(a)} + \mathcal{A}_k^{(a)}) - \sum_{k=1}^{M-1} (e_{k,k+1} + e_{k+1,k}) \otimes \mathcal{B}_k^{(a)} \\ &= \begin{bmatrix} \mathcal{A}_0^{(a)} + \mathcal{A}_1^{(a)} & -\mathcal{B}_1^{(a)} & \mathbf{0} & \cdots & \mathbf{0} \\ -\mathcal{B}_1^{(a)} & \mathcal{A}_1^{(a)} + \mathcal{A}_2^{(a)} & -\mathcal{B}_2^{(a)} & \cdots & \mathbf{0} \\ \mathbf{0} & -\mathcal{B}_2^{(a)} & \mathcal{A}_2^{(a)} + \mathcal{A}_3^{(a)} & \ddots & \vdots \\ \vdots & \vdots & \ddots & \ddots & -\mathcal{B}_{M-1}^{(a)} \\ \mathbf{0} & \mathbf{0} & \cdots & -\mathcal{B}_{M-1}^{(a)} & \mathcal{A}_{M-1}^{(a)} + \mathcal{A}_M^{(a)} \end{bmatrix}, \end{aligned} \quad (\text{A12})$$

$$\mathcal{A}_k^{(a)} \equiv \sum_{n=1}^{2N} A_{n,k}^{(a)} \mathbf{v}_{n,k} \mathbf{v}_{n,k}^T, \quad \mathcal{B}_k^{(a)} \equiv \sum_{n=1}^{2N} B_{n,k}^{(a)} \mathbf{v}_{n,k} \mathbf{v}_{n,k}^T. \quad (\text{A13})$$

Here, $\mathcal{M}^{(a)}$ is a real symmetric block tridiagonal matrix, $e_{i,j}$ is the $M \times M$ matrix with 1 at the (i,j) -th entry with all other entries 0, \otimes is the Kronecker product of two matrices and $\mathcal{A}_k^{(a)}$ and $\mathcal{B}_k^{(a)}$ are $2N \times 2N$ matrices. [Note that in the present WC problem, one needs to project out two zero eigen-modes $\mathbf{v}_{n,k}$ (for each k) corresponding to uniform translations in the x and y directions; hence $\mathcal{A}_k^{(a)}$ and $\mathcal{B}_k^{(a)}$ become $(2N-2) \times (2N-2)$ matrices.]

In calculating $F[\mathbf{r}_0]$ —which essentially is the propagator of a quantum harmonic oscillator—with the same procedure, one merely substitutes $h_k \rightarrow h_0$ in every equa-

tion Eq. (A7–A13)

$$F[\mathbf{r}_0] = \left(\prod_{k=0}^M \prod_{n=1}^{2N} \sqrt{B_{n,k}^{(0)}} \right) \det(\mathcal{M}^{(0)})^{-\frac{1}{2}} \quad (\text{A14})$$

$$A_{n,k}^{(0)} \equiv \frac{\omega_{n,0}}{\tanh(\omega_{n,0} \Delta \tau_k)}, \quad B_{n,k}^{(0)} \equiv \frac{\omega_{n,0}}{\sinh(\omega_{n,0} \Delta \tau_k)}, \quad (\text{A15})$$

$$\mathcal{A}_k^{(0)} \equiv \sum_{n=1}^{2N} A_{n,k}^{(0)} \mathbf{v}_{n,0} \mathbf{v}_{n,0}^T, \quad \mathcal{B}_k^{(0)} \equiv \sum_{n=1}^{2N} B_{n,k}^{(0)} \mathbf{v}_{n,0} \mathbf{v}_{n,0}^T, \quad (\text{A16})$$

$$\mathcal{M}^{(0)} \equiv \sum_{k=1}^M e_{k,k} \otimes (\mathcal{A}_{k-1}^{(0)} + \mathcal{A}_k^{(0)})$$

$$- \sum_{k=1}^{M-1} (e_{k,k+1} + e_{k+1,k}) \otimes \mathcal{B}_k^{(0)}. \quad (\text{A17})$$

Therefore,

$$\frac{F[\mathbf{r}^{(a)}(\tau)]}{F[\mathbf{r}_0]} = \left(\prod_{k=1}^{M-1} \prod_{n=1}^{2N} \frac{B_{n,k}^{(a)}}{B_{n,k}^{(0)}} \right)^{\frac{1}{2}} \left[\frac{\det(\mathcal{M}^{(a)})}{\det(\mathcal{M}^{(0)})} \right]^{-\frac{1}{2}}. \quad (\text{A18})$$

Here the product over k runs only from 1 to $M-1$ because the end interval contributions ($k = 0, M$) of $B_{n,k}^{(a)}$ and $B_{n,k}^{(0)}$ are identical although they formally approach 0 as $\tilde{\beta} \rightarrow \infty$ [since $\Delta\tau_{0,M} \rightarrow \infty$]. Similarly, one takes $A_{n,0}^{(a)} = A_{n,0}^{(0)} = A_{n,M}^{(a)} = A_{n,M}^{(0)} = \omega_{n,0}$ in calculating $\det \mathcal{M}$, as

$\Delta\tau \rightarrow \infty$ [since $\tanh(\omega_{n,0}\Delta\tau) \rightarrow 1$].

Finally, one needs to divide Eq. A18 by the (formally diverging) zero mode contribution to $F[\mathbf{r}^{(a)}(\tau)] = \det(-\partial_\tau^2 + V''[\mathbf{r}^{(a)}(\tau)])^{-1/2}$. For this, we numerically find the smallest λ such that

$$\frac{1}{F_\lambda[\mathbf{r}^{(a)}(\tau)]} \equiv \det(-\partial_\tau^2 + V''[\mathbf{r}^{(a)}(\tau)] - \lambda)^{\frac{1}{2}} = 0, \quad (\text{A19})$$

where the left hand side is calculated similarly as in Eqs. (A7–A13) with the substitution $V''(\mathbf{r}_k) \rightarrow V''(\mathbf{r}_k) - \lambda$. The fluctuation determinant is then obtained as

$$A_a = \sqrt{\lambda} \cdot \frac{F[\mathbf{r}^{(a)}(\tau)]}{F[\mathbf{r}_0]}. \quad (\text{A20})$$

-
- [1] E. Wigner, On the interaction of electrons in metals, *Phys. Rev.* **46**, 1002 (1934).
 - [2] B. Tanatar and D. M. Ceperley, Ground state of the two-dimensional electron gas, *Physical Review B* **39**, 5005 (1989).
 - [3] C. Attacalite, S. Moroni, P. Gori-Giorgi, and G. B. Bachelet, Correlation energy and spin polarization in the 2D electron gas, *Physical Review Letters* **88**, 256601 (2002).
 - [4] N. Drummond and R. Needs, Phase diagram of the low-density two-dimensional homogeneous electron gas, *Physical Review Letters* **102**, 126402 (2009).
 - [5] M. S. Hossain, M. Ma, K. V. Rosales, Y. Chung, L. Pfeiffer, K. West, K. Baldwin, and M. Shayegan, Observation of spontaneous ferromagnetism in a two-dimensional electron system, *Proceedings of the National Academy of Sciences* **117**, 32244 (2020).
 - [6] M. S. Hossain, M. Ma, K. Villegas-Rosales, Y. Chung, L. Pfeiffer, K. West, K. Baldwin, and M. Shayegan, Spontaneous valley polarization of itinerant electrons, *Physical Review Letters* **127**, 116601 (2021).
 - [7] K.-S. Kim and S. A. Kivelson, Discovery of an insulating ferromagnetic phase of electrons in two dimensions, *Proceedings of the National Academy of Sciences* **118** (2021).
 - [8] J. Falson, I. Sodemann, B. Skinner, D. Tabrea, Y. Kozuka, A. Tsukazaki, M. Kawasaki, K. von Klitzing, and J. H. Smet, Competing correlated states around the zero-field Wigner crystallization transition of electrons in two dimensions, *Nature Materials* **21**, 311 (2022).
 - [9] B. Bernu, L. Cândido, and D. M. Ceperley, Exchange frequencies in the 2D Wigner crystal, *Phys. Rev. Lett.* **86**, 870 (2001).
 - [10] B. Spivak and S. A. Kivelson, Transport in two dimensional electronic micro-emulsions, *Annals of Physics* **321**, 2071 (2006).
 - [11] M. Roger, Multiple exchange in ^3He and in the Wigner solid, *Phys. Rev. B* **30**, 6432 (1984).
 - [12] M. Roger, J. Hetherington, and J. Delrieu, Magnetism in solid ^3He , *Reviews of Modern Physics* **55**, 1 (1983).
 - [13] S. Chakravarty, S. Kivelson, C. Nayak, and K. Voelker, Wigner glass, spin liquids and the metal-insulator transition, *Philosophical Magazine B* **79**, 859 (1999).
 - [14] M. Katano and D. S. Hirashima, Multiple-spin exchange in a two-dimensional Wigner crystal, *Phys. Rev. B* **62**, 2573 (2000).
 - [15] K. Voelker and S. Chakravarty, Multiparticle ring exchange in the Wigner glass and its possible relevance to strongly interacting two-dimensional electron systems in the presence of disorder, *Physical Review B* **64**, 235125 (2001).
 - [16] K.-S. Kim, C. Murthy, A. Pandey, and S. A. Kivelson, Interstitial-induced ferromagnetism in a two-dimensional Wigner crystal, *Physical Review Letters* **129**, 227202 (2022).
 - [17] There is a sign error in the correlated hopping terms t_2 and t'_2 in Eq. (4) of Ref. [16], which led the authors to erroneously claim that the interstitial dynamics induces a fully-polarized ferromagnet. This is corrected as in Eq. (18) of the current paper. The resulting magnetism due to the interstitial dynamics is more complicated as discussed in Sec. V.
 - [18] D. S. Fisher, B. I. Halperin, and R. Morf, Defects in the two-dimensional electron solid and implications for melting, *Phys. Rev. B* **20**, 4692 (1979).
 - [19] E. Cockayne and V. Elser, Energetics of point defects in the two-dimensional Wigner crystal, *Phys. Rev. B* **43**, 623 (1991).
 - [20] Note that the energetics of these point defects are also studied using the path integral Monte Carlo method in Ref. [55], but the contributions from defect hopping and exchange processes are ignored.
 - [21] When considering exchange processes in a pure WC, V_0 corresponds to the classical WC energy. For tunneling processes involving a defect, V_0 corresponds to the classical energy of the defect.
 - [22] D. Thouless, Exchange in solid ^3He and the Heisenberg Hamiltonian, *Proceedings of the Physical Society* (1958-1967) **86**, 893 (1965).
 - [23] S. Coleman, *Aspects of symmetry: selected Erice lectures*, Cambridge University Press (1988).
 - [24] A. Altland and B. D. Simons, *Condensed matter field theory*, Cambridge University Press (2010).
 - [25] J. Zinn-Justin, *Quantum field theory and critical phe-*

- nomena*, Oxford University Press (2021).
- [26] The interaction between defects is small in proportion to a polynomial power of $1/d$, where d is the distance between them, and can be neglected if the defect concentration is dilute enough.
 - [27] Note that the tunnel barrier for t_{11} is anomalously smaller than that for any other processes, implying that the dynamics of the vacancy is predominantly unidirectional in the $r_s \rightarrow \infty$ limit. Such a peculiar defect dynamics has also been predicted to occur in solid helium [56]. Such a “restricted mobility” would in turn lead to an exponentially slow (in $\sqrt{r_s}$) thermalization in the presence of a dilute vacancy concentration. However, within the semi-classical approximation, t_{11} is the largest energy scale only when $r_s \gtrsim 320$, and this peculiar feature may be difficult to observe in practice.
 - [28] E. Eisenberg and E. H. Lieb, Polarization of interacting bosons with spin, *Physical review letters* **89**, 220403 (2002).
 - [29] K. Yang and Y.-Q. Li, Rigorous proof of pseudospin ferromagnetism in two-component bosonic systems with component-independent interactions, *International Journal of Modern Physics B* **17**, 1027 (2003).
 - [30] We note that the semi-classical expressions for many dynamical processes considered in this paper may not be taken at their face value in the range $r_s \lesssim 100$, as the instanton approximation breaks down when $\sqrt{r_s}S_a \lesssim 1$. For example, for $S_{t_1} = 0.098$ and $r_s = 100$, $\sqrt{r_s}S_{t_1} = 0.98 \lesssim 1$.
 - [31] Our results for $C_{1,i}$ and $C_{3/2,i}$ agree with Ref. [19]. Note the factor 2 difference between our values and those of Ref. [19] due to the difference in the unit of energy.
 - [32] Our calculation is performed in a hexagonal supercell as opposed to that of Ref. [19] in a rectangular supercell.
 - [33] The possibility of a quantum crystal in which the particle density per crystalline unit cell is different from an integer value was originally conceived of in Ref. [57] in the context of solid helium.
 - [34] H. Falakshahi and X. Waintal, Hybrid phase at the quantum melting of the Wigner crystal, *Physical Review Letters* **94**, 046801 (2005).
 - [35] D. P. Arovas, E. Berg, S. A. Kivelson, and S. Raghu, The Hubbard model, *Annual Review of Condensed Matter Physics* **13**, 239 (2022).
 - [36] V. Emery, S. Kivelson, and H. Lin, Phase separation in the $t - J$ model, *Physical Review Letters* **64**, 475 (1990).
 - [37] E. Eisenberg, R. Berkovits, D. A. Huse, and B. Altshuler, Breakdown of the Nagaoka phase in the two-dimensional $t - J$ model, *Physical Review B* **65**, 134437 (2002).
 - [38] This argument ignores a subtlety regarding the formation of mesoscale density-modulated “microemulsion” phases in a (possibly narrow) regime about any putative first-order transition in the presence of Coulomb interactions [10, 58–60].
 - [39] Note, however, that even if the self-doping transition occurs in the spinful problem, it need not occur in the spinless problem if the spinless (or fully-polarized) MeC phase always has higher energy than both the fully-polarized WC and a fully-polarized FL.
 - [40] The potential importance of defect hopping processes in the magnetism of a quantum crystal was pointed out earlier in Refs. [22, 42, 61]. For a comprehensive discussion in the context of solid ^3He , see [62].
 - [41] Such a spin-polaron is also shown to occur in the triangular lattice Hubbard model in the presence of a large Zeeman field [63, 64].
 - [42] B. Spivak and F. Zhou, Ferromagnetic correlations in quasi-one-dimensional conducting channels, *Physical Review B* **61**, 16730 (2000).
 - [43] J. O. Haerter and B. S. Shastry, Kinetic antiferromagnetism in the triangular lattice, *Physical Review Letters* **95**, 087202 (2005).
 - [44] C. N. Sposetti, B. Bravo, A. E. Trumper, C. J. Gazza, and L. O. Manuel, Classical antiferromagnetism in kinetically frustrated electronic models, *Physical Review Letters* **112**, 187204 (2014).
 - [45] Z. Zhu, D. Sheng, and A. Vishwanath, Doped Mott insulators in the triangular-lattice Hubbard model, *Physical Review B* **105**, 205110 (2022).
 - [46] K.-S. Kim, Exact hole-induced resonating-valence-bond ground state in certain $U = \infty$ Hubbard models, *Physical Review B* **107**, L140401 (2023).
 - [47] K.-S. Kim and H. Katsura, Exact hole-induced $SU(N)$ flavor-singlets in certain $U = \infty$ $SU(N)$ Hubbard models, *arXiv preprint arXiv:2307.09500* (2023).
 - [48] Y. Tang, L. Li, T. Li, Y. Xu, S. Liu, K. Barmak, K. Watanabe, T. Taniguchi, A. H. MacDonald, J. Shan, and K. F. Mak, Simulation of Hubbard model physics in WSe_2/WS_2 Moiré superlattices, *Nature* **579**, 353 (2020).
 - [49] Y. Xu, S. Liu, D. A. Rhodes, K. Watanabe, T. Taniguchi, J. Hone, V. Elser, K. F. Mak, and J. Shan, Correlated insulating states at fractional fillings of Moiré superlattices, *Nature* **587**, 214 (2020).
 - [50] E. C. Regan, D. Wang, C. Jin, M. I. Bakti Utama, B. Gao, X. Wei, S. Zhao, W. Zhao, Z. Zhang, K. Yumigeta, M. Blei, J. D. Carlström, K. Watanabe, T. Taniguchi, S. Tongay, M. Crommie, A. Zettl, and F. Wang, Mott and generalized Wigner crystal states in WSe_2/WS_2 Moiré superlattices, *Nature* **579**, 359 (2020).
 - [51] N. Morales-Durán, A. H. MacDonald, and P. Potasz, Metal-insulator transition in transition metal dichalcogenide heterobilayer Moiré superlattices, *Phys. Rev. B* **103**, L241110 (2021).
 - [52] Y. Yang, M. Morales, and S. Zhang, Metal-insulator transition in transition metal dichalcogenide heterobilayer: accurate treatment of interaction (2023), *arXiv:2306.14954 [cond-mat.str-el]*.
 - [53] This explanation for unexpectedly robust insulating magnetism is distinct from, although related to, a previous proposal [16] based on WC-FL puddle formation.
 - [54] P. K. Mogensen and A. N. Riseth, Optim: A mathematical optimization package for Julia, *Journal of Open Source Software* **3**, 615 (2018).
 - [55] L. Cândido, P. Phillips, and D. Ceperley, Single and paired point defects in a 2d Wigner crystal, *Physical review letters* **86**, 492 (2001).
 - [56] A. F. Andreev, Diffusion in quantum crystals, *Soviet Physics Uspekhi* **19**, 137 (1976).
 - [57] A. F. Andreev and I. M. Lifshitz, Quantum Theory of Defects in Crystals, *Soviet Journal of Experimental and Theoretical Physics* **29**, 1107 (1969).
 - [58] B. Spivak, Phase separation in the two-dimensional electron liquid in MOSFET’s, *Physical Review B* **67**, 125205 (2003).
 - [59] B. Spivak and S. A. Kivelson, Phases intermediate between a two-dimensional electron liquid and Wigner crystal, *Physical Review B* **70**, 155114 (2004).
 - [60] R. Jamei, S. Kivelson, and B. Spivak, Universal aspects

- of Coulomb-frustrated phase separation, *Physical Review Letters* **94**, 056805 (2005).
- [61] B. Castaing and P. Nozières, Phase transitions of spin polarized ^3He : a thermodynamical nuclear orientation technique?, *Journal de Physique* **40**, 257 (1979).
- [62] G. Montambaux, M. Heritier, and P. Lederer, Vacancies in a quantum crystal of fermions. the spin polaron in solid ^3He , *Journal of Low Temperature Physics* **47**, 39 (1982).
- [63] M. Davydova, Y. Zhang, and L. Fu, Itinerant spin polaron and metallic ferromagnetism in semiconductor Moiré superlattices, *Physical Review B* **107**, 224420 (2023).
- [64] S.-S. Zhang, W. Zhu, and C. D. Batista, Pairing from strong repulsion in triangular lattice hubbard model, *Physical Review B* **97**, 140507 (2018).